Open access • Journal Article • DOI:10.1109/JLT.2005.849945

Nonsilica glasses for holey fibers — **Source link** ↗

Xian Feng, A.K. Mairaj, Daniel W. Hewak, Tanya M. Monro

Institutions: University of Southampton

Topics: Optical fiber

Related papers:

- All-silica single-mode optical fiber with photonic crystal cladding

- Photonic crystal fibers

- Endlessly single-mode photonic crystal fiber.

- Supercontinuum generation in photonic crystal fiber

- Bismuth glass holey fibers with high nonlinearity

Nonsilica Glasses for Holey Fibers

Xian Feng, Arshad K. Mairaj, Daniel W. Hewak, and Tanya M. Monro

Abstract—The authors of this paper investigated the thermal properties and optical properties of typical nonsilica glasses, including viscosity, surface tension, thermal conductivity, transmission, linear and nonlinear refractive index, and fiber attenuation in order to judge the feasibility of using nonsilica glasses as the background material of holey fibers (HFs). Novel techniques were presented to fabricate the nonsilica glass microstructured fiber preforms. Examples of fabricated nonsilica glass HFs with various promising optical applications were finally exhibited.

Index Terms—Holey fibers (HFs), optical fiber fabrication, photonic-crystal fibers (PCFs).

I. INTRODUCTION

THE invention of holey fiber (HF) [1], [39], which is also known as the photonic-crystal fiber (PCF) or microstructured optical fiber (MOF), has attracted wide interest. HF is single-material-based optical fiber with air-filled holes surrounding the core along the entire length. Index guiding and bandgap guiding are the guiding mechanisms for high-index core HF and hollow-core (or low-index-core) HF, respectively. The combination of 1) the wavelength-scaled features of the air-filled holey cladding and 2) the high index contrast between the background material and the air is responsible for the unique optical performance of HFs, such as photonic bandgaps [2], large-mode area (LMA) with single-mode operation [3], high nonlinearity, supercontinuum generation, soliton effects [4]–[6], polarization maintenance, high birefringence [7], and dispersion management [8]. Various novel applications have been achieved in this new type of optical fiber.

As one of the candidates for the background material of HF, nonsilica glasses, including chalcogenide glasses, tellurite glasses, and other heavy metal oxide glasses, show unique advantages over the commonly used fused pure silica. Typically, nonsilica glasses possess the following qualities [9]:

1) highly linear refractive index n and nonlinear refractive index n;
2) high transparency from the near-infrared (near-IR) to the mid-IR region;
3) high rare-earth solubility;
4) low phonon energy, and so on.

Thus, nonsilica glass HF was proposed as a noteworthy candidate for highly nonlinear applications, novel devices for mid-IR laser transmission [10], and short active fiber devices.

Capillary-stacking techniques [10] and the extrusion technique [11] have already been utilized for making nonsilica glass HFs. The first single-mode nonsilica glass HF [11] and the world highest nonlinearity in optical fibers 640 $W^{-1}km^{-1}$ [12] were reported in the extruded HFs based on Schott SF57 glass (lead-silicate (PbO–SiO$_2$) glass). Supercontinuum generation, i.e., the broadening of the ultrashort pulse signal after passing through a nonlinear media, was also demonstrated in an extruded nonsilica glass HF based on Schott SF6 glass [13]. In addition, because nonsilica glasses typically possess higher refractive indexes ($n = 1.5 \sim 2.8$) than that of pure silica glass ($n = 1.44$), photonic bandgaps can be observed in bandgap HFs based on high-index nonsilica glass [14]. Bandgap guiding in nonsilica glass HF was first reported in the so-called omniguide fiber, in which a hollow core is surrounded by an alternating cladding of high- and low-refractive-index layers composed of AsSe$_3$ glass ($n = 2.8$) and a thermoplastic polymer, polyether sulphone (PES) ($n = 1.55$), respectively [15]. Using nonsilica glasses such as chalcogenide glasses, which have high index ($n = 2.0$–2.8) and high transparency in mid-IR regions (2–10 μm), very broad bandgaps in the mid-IR region was predicted in hollow-core bandgap HFs for the potential applications for IR laser transmission [15]. Since the light is mainly confined in the air-filled hollow core, the nonlinear effect under high power can be avoided, and the propagation attenuation of the light can even be lower than the selected background material of the fiber [15].

In the development of HFs, fiber fabrication is the most challenging aspect, compared with the work of modeling, optical characterization, and device making. During the fiber drawing, the air-filled microstructured cladding will be deformed, due to the effects of the air pressure ($\boldsymbol{p}$) inside the air-filled holes, the surface tension ($\boldsymbol{\sigma}$) of the glass, and the temperature gradient ($\boldsymbol{T}$) in the microstructured fiber preform (see Fig. 1). In order to minimize the collapse of the holey cladding when drawing fibers, all the holes in the preform normally need to be sealed before fiber drawing. Therefore, the air pressure inside the holey structure increases gradually during fiber drawing because of the decrease in the internal volume of the air-filled holes ($\boldsymbol{V_{in}}$). These ever-changing variables make it difficult to fabricate tens-of-kilometers-long HFs with identical and controllable cladding configurations. As the result, the deformation of the microstructured cladding of HFs is not only dimension dependent but also time dependent during fiber drawing. All the above variables need to be evaluated when selecting the background material for the HF.

In this paper, a wide range of investigation concerning the material properties of nonsilica glasses and the fabrication techniques of nonsilica glass HF has been initially performed. Examples of the fabricated HFs based on various nonsilica glasses have been exhibited finally.
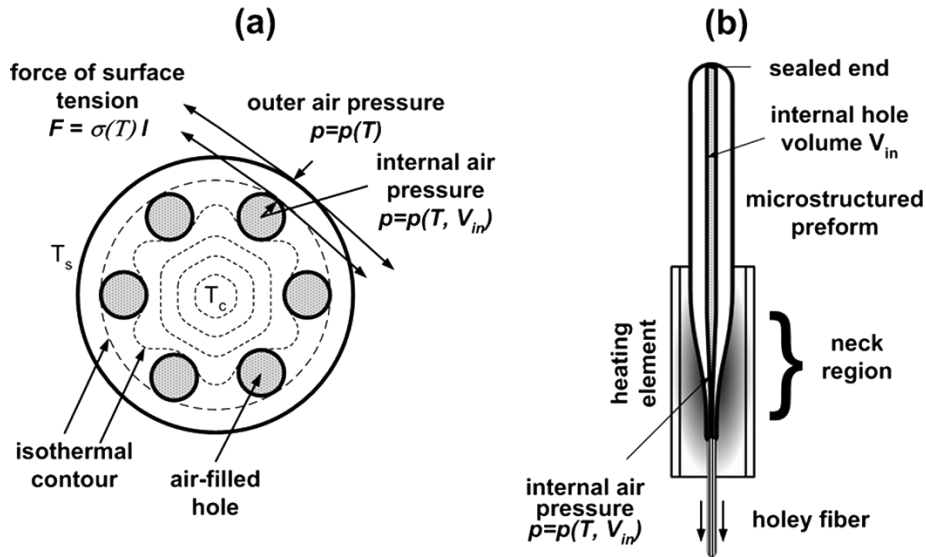
Fig. 1. Schematic diagram of temperature distribution, surface tension, and air pressure inside a simplified microstructured preform during drawing HF. It is assumed here that the circular preform is concentric with the circular temperature profile of the hotzone. (T_s is temperature on the outer surface of preform, and T_c is the temperature at the center of the preform.) (a) Cross-sectional view. (b) Vertical view.

II. EXPERIMENTAL PROCEDURES

Typical nonsilica glasses, such as high-lead silicate (SiO_2–PbO) glass (commercial Schott SF57 and SF59), tellurite glass ($75TeO_2$–$20ZnO$–$5Na_2O$), mol%), and gallium lanthanum chalcosulfide glass (GLS, $65Ga_2S_3$–$32La_2S_3$–$3La_2O_3$, mol%) were selected. The viscosities of the studied glasses were determined through the parallel plate method [16]. A commercial thermal–mechanical analyzer, a Perkin-Elmer TMA 7, with a high displacement sensitivity (up to 50 nm) and temperature range up to 1000 °C, was used to measure the glass viscosity from 10^5 to 10^8 poise (1 poise = 0.1 Pa · s).

The transmission spectra of the polished bulk glasses were measured by a Cary 500 Scan UV-VIS-NIR spectrophotometer from 190 to 2500 nm and by a Perkin–Elmer system 2000 FTIR (Fourier transform infrared) spectrophotometer from 2.5 to 25 μm (i.e., 4000–400 cm^{-1}), respectively.

For the measurement of the fiber attenuation in the near-IR region, a tungsten halogen lamp (0.25–2.5 μm) was used as the light source, and an optical spectrum analyzer (Ando AQ-6315A) was used to record the transmission spectra from 600 to 1700 nm. For the measurement of the fiber attenuation in the mid-IR region, a Perkin–Elmer system 2000 FTIR spectrophotometer was used to measure the fiber losses from 1.0 to 5.0 μm (i.e., 10 000–2000 cm^{-1}), using a liquid-nitrogen-cooled MCT (HgCdTe) detector.

A UMT-7 rotary sonic drilling machine (made by Branson Sonic Power) was utilized in drilling holey microstructured preforms. The rotary ultrasonic motion with the assistance of the coolant flow produces a self-cleaning action that reduces diamond tool binding. Therefore, this technique is particularly useful for machining hard and brittle materials such as ceramics, glasses, ferrite, and similar materials [17]. With the assistance of a micrometer, the drilled holes in the preforms can be precisely located with the deviation less than 20 μm/cm along the axial direction and less than 20 μm along the radial direction on the preform.

A custom-designed extrusion apparatus, which consists of an oil hydraulic press and a high-temperature furnace providing up to 4 tons of force with the upper operating temperature of 750 °C, was used in extruding microstructured holey preforms. The starting glass disk has a diameter of 30 mm and a height of 20–35 mm. After being heated to the temperatures corresponding to the glass viscosity range of $10^9 - 10^7$ poise, the solid-state glass is softened into the viscoelastic flow so that the preform with the desired microstructure can be fabricated after the glass flow is extruded through the structured die.

The fibers were drawn in a custom-designed fiber-drawing tower. Using a radio-frequency-induced heating furnace, the heating and cooling rates for fiber drawing can be as fast as 100 °C/min. Various atmospheres such as argon (Ar), nitrogen (N_2), and oxygen (O_2) can be purged inside the furnace, according to requirements of the selected glass.

The cross-sectional profiles of the fabricated HFs were observed using an analytical scanning electron microscope (SEM) (LEO 430, Cambridge, U.K.) with a resolution of 5 nm.

A COHU 7512 charge-coupled device (CCD) camera was used with Spiricon LBA-PC v 3.23 software (Spiricon Inc., Logan, UT) for imaging the near-field beam profile from the output end of the fiber.

III. MATERIAL PROPERTIES

A. Viscosity and Surface Tension

Fig. 2 shows the measured viscosity curves of some studied glasses, including the commercial Schott SF59 glasses (SiO_2–B_2O_3–PbO, PbO > 60 mol%), and the homemade tellurite glass ($75TeO_2$–$20ZnO$–$5Na_2O$, mol%) and GLS glasses ($65Ga_2S_3$–$32La_2S_3$–$3La_2O_3$, mol%). The viscosity data have been extrapolated to $10^{3.5}$ poise, according to the Arrhenius viscosity formula [18]: $\eta = \eta_0 \exp(-E_\eta/RT)$, where η is the viscosity, E_η the activation energy for viscous flow, R the gas constant, and T the absolute temperature of the glass
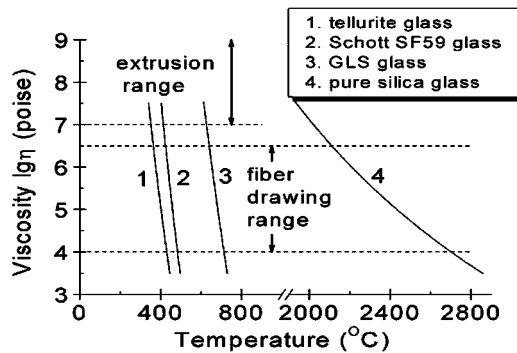
Fig. 2. Viscosity of some studied glasses: 1) tellurite glass ($75TeO_2$–$20ZnO$–$5Na_2O$, mol%), 2) Schott SF59 glass (lead borosilicate glass), 3) GLS glass ($65Ga_2S_3$–$32La_2S_3$–$3La_2O_3$, mol%), and 4) pure silica glass [19].

flow (Kelvin). The viscosity curve of pure silica glass is also illustrated in Fig. 2, according to [19]. It is seen that nonsilica glasses typically have steep viscosity curves, and the operating range for fiber drawing is less than 100 °C, while pure silica glass has a flat viscosity curve, and the operating temperature range for fiber drawing is as wide as 600 °C. Essentially, in order to minimize the temperature gradient on the holey cladding of the preform and to avoid the phase separation and thermal crystallization of the nonsilica glasses during drawing fiber, it is always necessary to maintain the fiber-drawing temperature at relatively low temperature, which corresponds to the viscosity range of $\sim 10^5 - 10^{6.5}$ poise. Therefore, the processing temperature suitable for drawing nonsilica glass HFs is indeed much narrower than silica HFs.

It has been known that the molar surface tension of the glass modifier ions drops dramatically with the increase of the ionic potential Z/r (Z is the charge of ion, and r is the ion radius) [20]. Since typical nonsilica glasses contain a large fraction of heavy-metal ions to stabilize the glass thermal stability and extend the transmission to mid-IR and increase the linear refractive and nonlinear refractive index, they have the surface tension lower than pure silica by one or two magnitudes. It can be deduced that the air pressure (p) (see Fig. 1) in the holey structure and the temperature gradient in the preform are the dominant factors during drawing nonsilica glass HFs, which is different from drawing silica HFs.

B. Transmission and Thermal Conductivity

Fig. 3(a) shows the measured transmission spectra of commercial Schott SF59 glass (SiO_2–B_2O_3–PbO, $PbO > 80$ wt%), the homemade GLS glass ($65Ga_2S_3$–$32La_2S_3$–$3La_2O_3$, mol%) and tellurite glass ($75TeO_2$–$20ZnO$–$5Na_2O$, mol%), and pure silica glass. Pure silica glass shows high transparency from 250 to 2500 nm so that it should be extremely promising for the optical applications from the ultraviolet (UV) region ($< 0.4~\mu$m) to the near-IR region. Chalcosulfide glass can be highly transparent up to 9 μm, indicating its promising potential in the mid-IR region (3–10 μm). Tellurite glass can essentially satisfy the requirements for the applications from 1.0 to 3.0 μm. What is more, assuming the fundamental vibration of the hydrogen-bonding absorption band between 3 and 4 μm [21] can be removed from the glass by improving the melting conditions,

tellurite glass can even be utilized up to a wavelength of 4–5 μm. High-lead silicate glass (Schott SF59) shows inferior in the visible region (0.4–0.7 μm) to silica and also shows inferior in the mid-IR region to chalcosulfide glass and tellurite glass so that their applications can only be limited within the near-IR range (1.0–1.6 μm).

Air, one type of the well-known poor thermal conductors, has the thermal conductivity of only ~ 0.06 $Wm^{-1}K^{-1}$ at 600 °C, which is less than that of glass materials by one order of magnitude [22]. During drawing HF, the air-filled holey array will isolate most of the heat conducted from the outer side of the preform toward the center along the radial direction, and only the glass bridges between the adjacent holes can conduct the heat [see Fig. 1(a)]. Consequently, one must be aware of the situation of heat transfer in the air-filled microstructured preform to suitably adjust the processing conditions when drawing the HF based on a certain type of nonsilica glass. Hence, the thermal conductivity is one of the most useful parameters required to fabricate the desired microstructured holey cladding. Unfortunately, it is one of the most difficult properties of optical glasses to be evaluated [23].

Generally, the heat can transfer through the glass by thermal conduction and radiant transfer. For a colorless glass, true thermal conduction is dominant at low temperatures, while radiant transfer becomes more important at high temperatures. Therefore, the concept of effective conductivity λ_{eff} was introduced [24]. It is defined by $\lambda_{\mathrm{eff}} = \lambda_0 + \lambda_R$, where λ_0 is the true conductivity, and λ_R, the radiation conductivity, can be calculated by $\lambda_R = (16/3)(n^2\sigma T^3/\alpha)$ (n is the refractive index of the medium, σ the Stefan–Boltzmann constant, and α the absorption coefficient of the material). The obvious difficulty for evaluating λ_R is that the coloring agents and the impurities such as iron make it strongly dependent on the wavelengths.

According to the Wien displacement law, the distribution function of the normalized black body radiation energy versus wavelength (λ) can be expressed as $\lambda T = k_i$, where k_i is a constant depending on the point on the spectrum. Above 300 °C, the radiation component of the transfer of heat in glasses begins to increase noticeably. For example, a significant fraction of the radiation may be transmitted by a colorless silicate glass at any temperature above 300 °C [23]. Thus, the effective conductivity appears steeply temperature dependent at high temperature, and it could be more than an order of magnitude greater than the true conductivity when above 1000 °C. For most nonsilica glasses, the fiber-drawing temperature is between 300 and 800 °C. Consequently, the radiation conduction is more important than the true conductivity during the drawing of nonsilica glass HFs.

Fig. 3(b) shows the function of radiation energy versus wavelength based on the assumption of the black body. The radiation near the peak wavelength possesses the principal portion of the total radiation energy, and the peak of the radiation energy shifts toward the short wavelengths with the increase of the temperature. Therefore, the transmission characteristics of optical glasses are important for radiation conduction. Two types of optical glasses here show a good match between the radiation conductivity at the fiber-drawing temperatures and their transmission windows. First, pure silica glass is extremely suitable to be drawn into HF because its fiber-drawing temperatures range
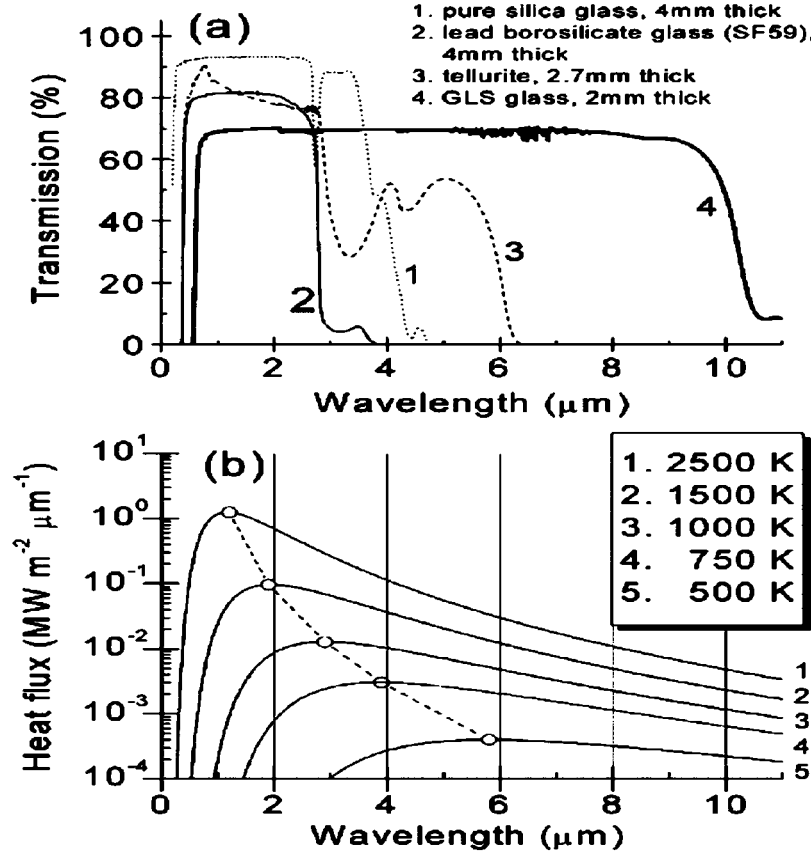
Fig. 3. (a) Transmission spectra of typical optical glasses: 1) pure silica (SiO_2) glass, 2) Schott SF59 (SiO_2–B_2O_3–PbO glass, PbO $>$ 60 mol%), 3) tellurite glass (75TeO_2–20ZnO–5Na_2O, mol%) made in the Optoelectronic Research Centre (ORC), University of Southhampton, and 4) GLS (65Ga_2S_3–32La_2S_3–3La_2O_3, mol%) made in ORC. (b) Relation of radiation energy versus wavelength based on black body.

between 2100 and 2700 °C (see Fig. 2), and pure silica glass is highly transparent from 2.5 μm to the UV region (200–400 nm). Second, chalcosulfide glasses are also suitable to be drawn into HFs because they are highly transparent from the near-IR to the mid-IR region (1–10 μm), and their fiber-drawing temperatures are normally between 350 and 800 °C (see Fig. 2). Lead-silicate glasses and tellurite glasses show somewhat inferior as the background materials of HFs, mainly due to the narrow transmission window and also partly due to strong OH absorption at 3–4 μm. At the high temperature when drawing fiber, the UV edge of the transmission spectrum will shift to the longer wavelengths and the transmission window becomes narrow so that the real situation when drawing fiber should be more complicated. Here we assume that transmission spectra of glass at high temperatures will not change too significantly compared to the transmission at room temperature, in order to make the discussion simple.

C. Refractive Index and Nonlinear Refractive Index

The large contrast of the refractive indexes between the background material and the air is one of the main reasons for the unique optical properties of HFs, such as photonic bandgap, dispersion flattening, endless single-mode guidance, and high confinement of light inside the core. The high nonlinear index of the background material is also one of the main factors to achieve high effective nonlinearity in the index-guided small-core HFs. The relationship between the linear refractive index

n_o and the nonlinear refractive index n_2 for an optical material are defined by $n(I) = n_o + n_2I$, where $n(I)$ is the total refractive index of the material, and I is the optical intensity (W/m^2) of the incident beam, respectively, applied with the laser wave [25], [26]. The unit of n_2 is m^2/W or, more customarily, cm^2/W. For a linear-polarized monochromatic beam of frequency ϖ and an isotropic medium, the nonlinear index of refraction n_2 is related to the real part of third-order susceptibility $\chi^{(3)}$ via $n_2 = (12\pi/n_0)\{\text{Re}\chi^{(3)}_{1111}(-\omega, \omega, \omega, -\omega)\}$, where $\text{Re}\chi^{(3)}_{1111}(-\omega, \omega, \omega, -\omega)$ is the real part of the diagonal element of the third-order susceptibility [27].

A semiempirical relationship was found between n_2 and the Abbe number ν_d and n_d [27], which has already been converted into SI units as follows:

$$n_2(10^{-13}\text{m}^2/\text{W})$$
$$= \frac{68 \times (n_d - 1) \cdot (n_d^2 + 2)^2}{2.387 \times 10^6 n_0 \cdot \nu_d \cdot \left[1.517 + \frac{(n_d^2+2)\cdot(n_d-1)\cdot\nu_d}{6n_d}\right]^{\frac{1}{2}}} \quad (1)$$

where c is the light speed in vacuum (3.0×10^8 m/s). This Boling–Glass–Owyoung (BGO) formula has already been demonstrated to match the measured values very well [27]. The relation between the refractive index n_d and the nonlinear refractive index n_2 in various optical glasses is illustrated in Fig. 4. Note that the values of n_2 of all the commercial Schott optical glasses are calculated using the BGO formula. For other
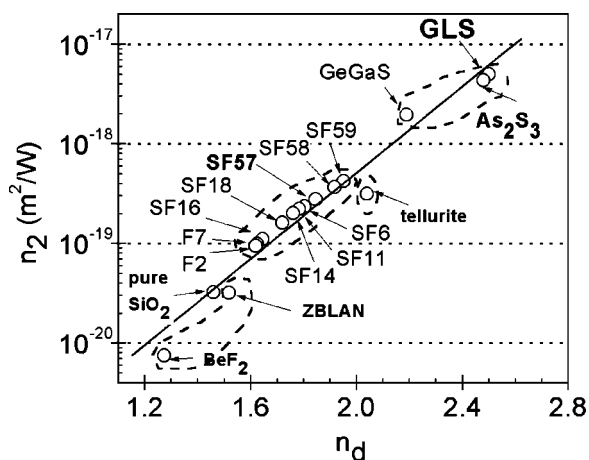
Fig. 4. Relation between refractive index n_d and nonlinear index n_2 of various optical glasses, including GLS glass [26], As_2S_3 glass [28], Ge–Ga–S glass [26], extremely heavy flint lead silicate glasses (Schott SF), flint (F) glasses, tellurite glass [9], fluoride glasses [19], and fused pure silica glass [29]. The straight line is fitted as the guiding line.
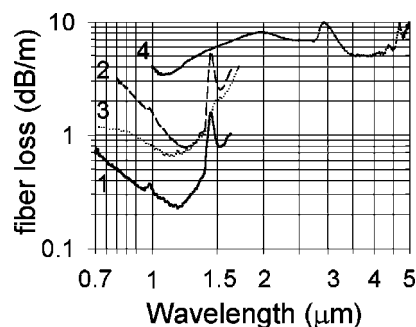

Fig. 5. Measured near-IR and mid-IR attenuation of unclad/unstructured fibers based on 1) Schott SF57 glass (lead silicate glass), 2) Schott SF59 glass (lead borosilicate glass), and 3) tellurite glass ($75TeO_2$–$20ZnO$–$5Na_2O$, mol%), and 4) GLS glass ($65Ga_2S_3$–$32La_2S_3$–$3La_2O_3$, mol%). Note that all fibers have the same diameter of $250 \pm 10 \mu m$.

glasses, including pure silica glass, fluoride glasses, tellurite glass, and chalcogenide glasses, the n_2s are cited based on [26], [28], and [29].

From the angle of the material chemistry, the linear refractive index and the nonlinear refractive index are both attributed to the polarizability and the hyperpolarizability of the constituent chemical ions. In conventional silicate glasses, network modifiers such as alkali oxide or alkali earth oxide increase the number of nonbridging oxygen atoms, which are more polarizable than the bridging oxygen atoms in the Si–O network, thus inducing a modest increase of the nonlinearity [30]. For the glasses with heavy-metal cations, the high nonlinearity is usually due to the hyperpolarizability of the constituent metal ions. For example, the lone 6-s electron pairs of Pb ions in PbO containing glasses are explained to be the cause of the high linear index and high nonlinear index [31]. Moreover, chalcogenide glasses composed mainly of chalcogens (S, Se, and Te) are among the most nonlinear glasses [28], because the larger hyperpolarizability of the S^{2-}, Se^{2-} and Te^{2-} ions than O^{2-} causes the higher linear index and nonlinear index of chalcogenide glasses than oxide glasses [32]. Fig. 4 is consistent with this explanation. It has been demonstrated that one can obtain a large n_2 by maximizing the linear refractive index n_0 and minimizing the two-photon-absorption (TPA) coefficient in the wavelength range of interest. Here, in order to simplify the complexity from the TPA, we just show the tendency of n_2 versus the n_d relation, which is sufficient in the essential requirement to seek the optical glasses with the highest nonlinear refractive index n_2. It is clear that the chalcosulfide glasses have not only the highest linear refractive index n_d but also the highest n_2 among all the studied glasses here. In order to further enhance the nonlinearity of glass, one can replace the sulfur in chalcogenide glasses by selenium or tellurium, which possesses higher hyperpolarizability than sulfur ions [28], although the resulted glass and fiber can only be used for the much longer wavelength ranges due to the red shift of the transmission window toward the long wavelengths.

D. Attenuation of Unclad/Unstructured Fibers

Fig. 5 illustrates the unclad/unstructured fibers based on the commercial Schott SF57 and SF59 glasses, and the homemade tellurite glass ($75TeO_2$–$20ZnO$–$5Na_2O$, mol%) and GLS glass ($65Ga2S_3$–$32La2S_3$$3La2O_3$, mol%). The preforms (rods and tubes) based on Schott glasses were cored directly from the commercial bulk glasses by ultrasonic drilling in order to shorten the thermal history processing the glass. Due to the flame polishing in the fiber- drawing, the surface roughness of the fiber was reduced to less than 10–20 nm/cm. The fiber attenuation arising from the scattering on the surface should be negligible. The tellurite glass rod was made by extrusion, while the GLS glass rod was cut from the melted glass ingot and then polished.

It is seen that the losses of Schott SF57 and SF59 glass unclad/unstructured fibers show the lowest values around 1.2 μm and increase to 1–3 dB/m at 1.55 μm due to the overtone of the fundamental vibration of hydrogen bonding at 3–3.5 μm. Although more lead-oxide (PbO) can be introduced into borosilicate glasses for higher linear and nonlinear refractive index, lead borosilicate glass (Schott SF59 glass, SiO_2– B_2O_3–PbO) fiber shows stronger OH absorption and consequently higher fiber attenuation at 1.5 μm than lead-silicate glass (Schott SF57 glass, SiO_2–PbO) fiber. It is mainly due to the hydrophilic nature of boron in the borosilicate glass.

GLS fiber shows only 3–5 dB/m between 1.0 and 1.6 μm without a significant trace of OH absorption, because of the extremely dry atmosphere used during glass melting and the hydrophobic nature of sulfide compounds. This type of glass fiber still shows the loss as low as 5 dB/m, even up to 4 μm, indicating its potentials in the mid-IR applications.

Tellurite glass fiber has the low loss of $\sim$0.7 dB/m at 1.1–1.3 μm, and its OH absorption around 1.4–1.5 μm is much weaker than that in Schott SF57 and SF59 fiber, although no particular dry atmosphere was used for melting tellurite glass. Due to the scattering centers generated during glass melting and extrusion, here the tellurite fiber still has higher loss than SF57 fiber. Tellurite glass fiber should have its own advantages for the applications from 1–3 μm.

TABLE I
COMPARISON OF OPTICAL GLASSES AS BACKGROUND MATERIAL

Glass System	Chalcogenide Glasses	Tellurite glasses	High Lead Silicate Glasses	Pure Silica Glass
Operating Temperature Range for Fiber-Drawing	<50 °C	<50 °C	<100 °C	>500 °C
Surface Tension	low	low	low	high
Transmission	0.5 - 10 μm	0.4-6μm	0.4 - 3 μm	0.2 - 3.5 μm
Radiation Conductivity	suitable for fiber-drawing at low temperature (300-800°C)	inferior to silica and chalcogenide glass	inferior to silica and chalcogenide glass	suitable for fiber-drawing at extremely high temperature (>2000 °C)
Refractive Index n	2.2-2.5 (or higher)	2.0-2.2	1.6-2.0 (or higher)	1.46
Nonlinear Refractive Index n_2	~100 times higher than pure silica glass	tens of times higher than pure silica glass	tens of times higher than pure silica glass	2.7×10^{-20} m²/W
Fiber Attenuation	3-5 dB/m at 1.0- 1.5μm, ~5dB/m at 4μm, low OH content	<1dB/m at 1.0 -1.3μm, low OH content	1-3 dB/m at 1.5μm, high OH content	<0.2dB/km @1.5μm

E. Comparison of Nonsilica Glasses as Background Material of Holey Fibers

Table I summarizes the thermal properties and optical properties of the studied nonsilica glasses. The thermal properties, such as viscosity and thermal conductivity, indicate that it is more difficult to fabricate nonsilica glass HF than silica HF. However, for some particular applications that silica HF cannot cover, such as extremely high nonlinear applications from 1 to 4 μm and mid-IR laser power delivery, nonsilica-glass-based HFs have the absolute advantages over silica HF.

Tellurite- and chalcogenide-glass-based HFs appear promising in the wide range from the near-IR to the mid-IR regime. In addition, one of the most challenging issues in the development of the chalcogenide glasses in the past decades is the very narrow glass forming region of chalcogenide glasses itself. It is extremely difficult to find one pair of glass compositions as the core and the cladding with the suitable index contrast, the sufficiently small thermal mismatch, and good thermal stability [33]. Therefore, the concept of single-material-based HFs appears particularly suitable for chalcogenide-glass-based optical fibers.

HFs based on commercial heavy-metal oxide (PbO and Bi_2O_3) containing silicate glasses can only be used within the range between 1 and 1.6 μm, due to the narrow transmission windows and the relatively high fiber attenuation. However, since they are commercially available and have the outstanding quality-to-cost ratio, it is worth developing commercial high-index oxide-glass-based HFs for cheap and short fiber devices but with sufficiently excellent optical performance.

IV. TECHNIQUES TO MANUFACTURE MICROSTRUCTURED HOLEY PREFORMS

A. Capillary Stacking

The capillary-stacking technique is the most commonly utilized technique to manufacture silica microstructured holey preforms [1], [39]. First, a commercial silica glass tube with 10–20-mm out diameter (OD) was elongated into ~1-mm-diameter capillaries. The capillaries were then stacked along with appropriately positioned solid glass rod(s). Thus, a microstructured holey preform with a cross section similarly reflecting the holey array required in the final fiber was created. A two-stage drawing process reduced the diameter of individual holes by a factor of ~10 000 to fabricate the HF. The prevailing advantage of this technique is the ability to manufacture microstructured preforms for the HFs with highly complex and periodic geometry, such as the hollow-core bandgap HFs, which need approximately ten rings of precisely periodic holey cladding structure [2]. For silica HF, low OH containing high-purity silica tubes with various ratios of inner diameter (ID) to OD is commercially available. It is convenient to elongate the silica tube into the capillary with the desired dimensions. However, for nonsilica glasses, it is difficult to find the widely available sources providing the glass tubes. Homemaking might be the only approach.

Fig. 6(a) shows the photograph of a stacked preform when it was necked down to 1.1-mm OD during the fiber drawing. A 3 wt% Nd_2O_3-doped Schott F7 glass was used as the core and undoped Schott F7 glass as the cladding ($n_D = 1.625$). An Nd-doped F7 rod and an undoped F7 tube were drilled from the commercial bulk glasses, and then they were elongated into the cane and capillary with uniform 600-μm OD. The capillary bundle was then stacked inside an undoped F7 glass tube and pulled into the fiber.

B. Extrusion

The extrusion technique has already been successfully applied in making microstructured holey preforms for glass HFs [11]–[13] and polymer HFs [34]. Under high pressure (typically $10^3 - 10^4$ N/cm²) and high temperature (corresponding to the viscosity range between 10^9 and 10^7 poise), the glass flow can be extruded through a microstructured die so that the preform with the designed holey microstructure can be fabricated. This technique is especially suitable for making glass workpieces based on those glasses with a short operating range (known as short glasses) or glasses with high tendency for crystallization [35]. It is indeed an efficient and economic way to fabricate the glass rods, tubes, and microstructured preforms with repeatable and controllable dimensions. An extruded GLS glass preform and a tellurite glass preform with simple microstructure are shown in Fig. 6(b). These preforms have the core diameter, spoke length, and spoke thickness of 1.9 mm, 5.9 mm, and 200 μm, respectively. In the HFs based on such a kind of microstructured cladding, the leakage losses from the solid core could be negligible compared with the inherent losses from the materials [11], [12]. The extremely large air-filling fraction efficiently confines the light mainly inside the core so that the extremely highly effective nonlinearity can be achieved in this type
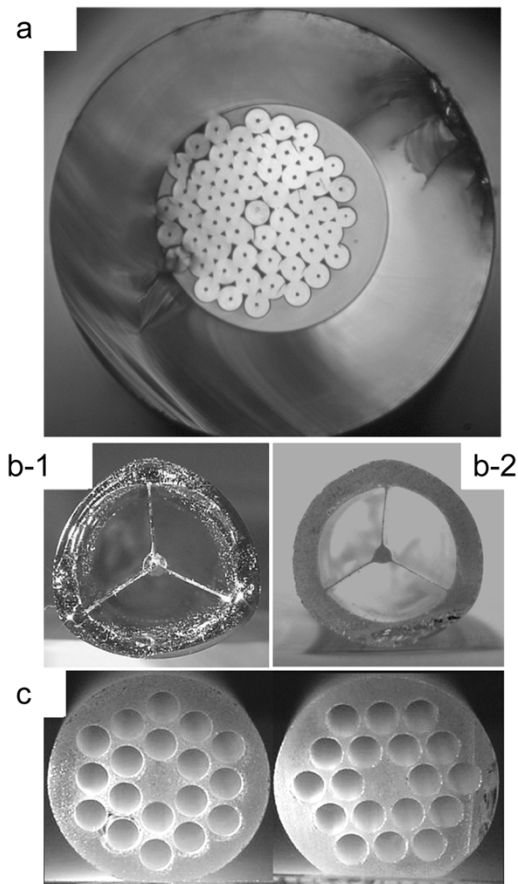
Fig. 6. (a) Necked cane from the preform by capillary stacking (OD: 1.1 mm, based on 3 wt% Nd_2O_3-doped Schott F7 as the core and undoped Schott F7 as the cladding). (b) Extruded microstructured preform based on (b-1) GLS ($65Ga_2S_3$–$32La_2S_3$–$3La_2O_3$, mol%) glass and (b-2) tellurite ($75TeO_2$–$20ZnO$–$5Na_2O$, mol%) glass made in our laboratory (core diameter: 1.9 mm, spoke length: 5.7 mm, and thickness: 0.2 mm). (c) Both cross-sectional views of a drilled microstructured preform based on high-lead silicate glass (Schott SF6): 18 holes with 2.40-mm ID holes and 400-μm hole spacing are periodically distributed on a 14-mm OD rod with the length of 60 mm.

TABLE II
SUMMARY OF TECHNIQUES MAKING MICROSTRUTURED PREFORMS

Technique	Stacking	Extrusion	Ultrasonic Drilling
Advantages and disadvantages	can achieve very *complex* microstructure (>100 holes)	particularly suitable for small core HF with *extremely large air-filled fraction*; so-far achieved structure with 12 holes [13]	particularly suitable for fabricate *precise* structure, but need long working time; so-far achieved structure with (but periodical) 18 holes (this work)
Human labor involved	high	low	low (if with automatic control)
Equipment cost	low	high	high

world's first man-made photonic bandgap crystal, by drilling on a block of dielectric material with a high refractive index of 3.6 [36]. Glass is one kind of well-known brittle material, which is strong in compression but weak in tension and bending. It tends to be broken by any tiny crack from the radial direction during drilling. If one wants to drill an array of dense and deep holes on the glass, say, the depth is more than 10 mm, and the wall thickness between the adjacent holes is less than 1 mm, the possibility for the cracking becomes high. At the early stage of the development of silica HFs, due to the quick success of the capillary-stacking technique, the drilling method finally vanished in fabricating the silica microstructured holey preforms.

However, with the assistance of the ultrasonic and/or sonic vibrations, the friction and pressure between the drill and the glass becomes much weak. Therefore, drilling deep holes in the glass preform should be possible. Second, with the assistance of the mechanical lathe, the position, the size, and even the angle of the holes on the glass preform can be controlled precisely. Here, we present a microstructured holey preform based on high-lead silicate glass (Schott SF6), using the ultrasonic drilling machine in our laboratory [see Fig. 6(c)]. The preform has 14-mm OD and 60-mm length. There are 18 identical holes with a 2.4-mm diameter periodically distributed on the two-ring triangular structure surrounding a solid core at the center. The thinnest part of the bridges between the adjacent holes is only 400 ± 20 μm thick. Although it took near ten hours to finish such a job, it is expected that a numerically controlled ultrasonic-drilling machine can fabricate glass preforms with a more complex holey array without so much involvement of human labor. There is no doubt that the drilling method can make the repeatable microstructure and can satisfy the requirements for the large-scale production of HFs. in addition, our experiments show that the surface roughness of the drilled preforms can be largely improved by flame polishing during fiber drawing or by chemical etching the drilled preforms before fiber drawing.

Table II summarizes the advantages and the disadvantages of the techniques manufacturing microstructured preforms for nonsilica glass HFs. By suitably selecting these technique(s), it is predicted that the ability of fabricating nonsilica glass HFs with relatively complex holey cladding can be largely enhanced and close to that of the current level of fabricating silica HFs.

of HF [12]. In addition, this type of microstructured preform with extremely thin microstructure cannot be fabricated by conventional methods such as glass molding [35].

However, by an extrusion technique, it is still quite challenging to fabricate the glass preforms with a very complex microstructure, say the triangular holey structure with more than three rings of holes. The thermomechanical strength of the die material is the main cause for this limitation. In addition, the thermal deformation of the preform, arising from the temperature gradient, the surface tension, and the turbulence of glass flow passing through the die make it somewhat difficult to achieve the microstructure in which each hole can be precisely positioned. In addition, the contamination from the surface of the metal die may also increase the attenuation of the resulted HFs.

C. Ultrasonic Drilling

Drilling is obviously a straightforward approach to manufacture the complex holey structure. Yablonovitch fabricated the
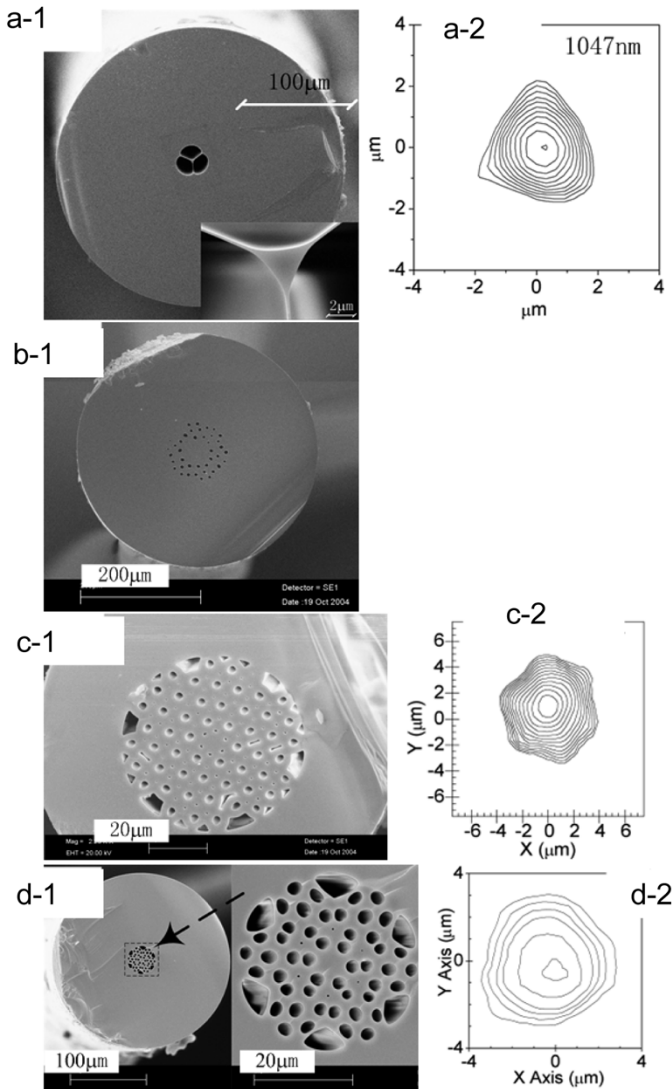
Fig. 7. (a) Fabricated small-core tellurite HF: (a-1) SEM photographs of the cross-sectional views and (a-2) single-mode guidance at 1047 nm. (b) Fabricated GLS LMA HF: (b-1) SEM photograph of the cross-sectional view. No guidance was observed due to the imperfect microstructured parameters. (c) Heavily Nd_2O_3-doped silicate glass (Schott F7) LMA HF for active device: (c-1) SEM photograph of the cross-sectional view and (c-2) single-mode guidance at 1047 nm with $A_{\rm eff}$ of $\sim 30\ \mu m^2$. (d) High-index-glass (Schott SF6)-based LMA HF for passive device: (d-1) SEM photographs of the cross-sectional views and (d-2) single-mode guidance at 800 nm with $A_{\rm eff}$ of $\sim 40\ \mu m^2$.

V. EXAMPLES OF FABRICATED NONSILICA HOLEY FIBERS

Based on the above investigation from the glass properties to the fabrication techniques, some nonsilica-glass-based HFs have been fabricated and are shown in Fig. 7.

Fig. 7(a-1) shows the SEM photographs of the cross-sectional views of a fabricated tellurite glass ($75TeO_2$–$20ZnO$–$5Na_2O$, mol%) HF with 250-μm OD. Extrusion technique was employed in the fabrication. Single-mode guidance was observed at 1047 nm in this fiber with $\sim 2.7\ \mu$m of core diameter. It is anticipated to observe highly effective nonlinearity in this fiber because of the small core size and the high nonlinearity of tellurite glass (see Fig. 4).

Fig. 7(b-1) shows a fabricated GLS HF with very large core diameter. Note that a desired one ring of holes around the core

completely collapsed during fiber drawing due to the improper fiber-drawing parameters. No guidance can be observed from this fiber since the holey cladding cannot confine for the light inside the core. The improvement of the fabrication is necessary.

Fig. 7(c-1) shows the SEM photo of a fabricated LMA HF based on Schott F7 glass ($n_D = 1.625$). Single-mode guidance is observed at 1047 nm [see Fig. 7(c-2)], and the effective-mode area $A_{\rm eff}(= [\int dr_\perp I(r_\perp)]^2 / \int dr_\perp I^2(r_\perp)$, where $I(r_\perp)$ is the intensity distribution [37]) was measured as 30 μm^2. Note that the core is heavily doped with 3 w.% of Nd_2O_3. The doping level of rare-earth ions in most of nonsilica glasses can be as high as 30 000–50 000 weight parts per million (wt ppm) without the significant concentration quenching, while in silica glass it can only be 1000–2000 wt ppm. Short active fiber devices with extremely LMA ($\gg 100\ \mu m^2$) with single-mode operation can be realized in this type of HF based on nonsilica glasses.

Fig. 7(d-1) gives the SEM photos of a fabricated LMA HF based on Schott SF6 glass ($n_D = 1.805$). Single-mode guidance was observed at 800 nm [see Fig. 7(d-2)] and the effective-mode area $A_{\rm eff}$ was measured as 40 μm^2. This type of passive LMA HF with single-mode operation is highly desired for delivering high power laser with excellent beam quality.

The examples in Fig. 7(b)–(d) were all fabricated by the capillary-stacking technique.

In addition, although HFs based on the typical nonsilica glasses can be fabricated successfully, the thermal properties of nonsilica glasses still make the fiber fabrication with large scale very difficult. The fabrication for all the above HFs has showed that it is difficult to fabricate the fiber with the enough length (>100–200 m) and without the significant deformation in the holey cladding, because the variables of drawing air-filled holey cladding is not only dimension dependent and but also time dependent (see Fig. 1). Since the key issue responsible for the novel optical performance of HFs is not the single material but the combination of the wavelength-scaled features and the high index contrast, all-solid microstructured optical fibers with high index contrast [38] could be a realistic solution to avoid such a problem.

VI. CONCLUSION

In summary, the authors have investigated a wide range from the glass thermal properties, optical properties, to the techniques fabricating the microstructured holey preforms of nonsilica glasses. Nonsilica glasses show advantageous optical properties over silica glass but are inferior to silica glass for the fabrication due to the limitation from the thermal properties of the nonsilica glasses. Examples of some fabricated nonsilica-glass-based HFs have been demonstrated, indicating the promising future of the HFs based on nonsilica glasses in the high nonlinear applications, the mid-infrared (IR) applications, and the compact active single-mode fiber devices with extremely large mode area (LMA), and so on.

REFERENCES

[1] J. C. Knight, T. A. Birks, P. S. J. Russell, and D. M. Atkin, "All-silica single-mode fiber with photonic crystal cladding," *Opt. Lett.*, vol. 21, pp. 1547–1549, 1996.

[2] J. C. Knight, J. Broeng, T. A. Birks, and P. S. J. Russell, "Photonic bandgap guidance in optical fibers," *Science*, vol. 282, pp. 1476–1478, 1998.

[3] J. C. Knight, T. A. Birks, R. F. Cregan, P. S. J. Russell, and J.-P. de Sandro, "Large mode area photonic crystal fiber," *Electron. Lett.*, vol. 34, pp. 1347–1348, 1998.

[4] T. M. Monro, D. J. Richardson, and N. G. R. Broderick, "Efficient modeling of holey fibers," presented at the Optical Fiber Commun. Conf., San Diego, CA, Feb. 21–26, 1999, Paper FG3.

[5] S. Coen, A. H. L. Chan, R. Leonhardt, J. D. Harvey, J. C. Knight, W. J. Wadsworth, and P. S. J. Russell, "White-light supercontinuum generation with 60-ps pump pulses in a photonic crystal fiber," *Opt. Lett.*, vol. 26, pp. 1356–1358, 2001.

[6] W. J. Wadsworth, J. C. Knight, A. Ortigosa-Blanch, J. Arriaga, E. Silvestre, and P. S. J. Russell, "Soliton effects in photonic crystal fibers at 850 nm," *Electron. Lett.*, vol. 36, pp. 53–55, 2000.

[7] A. Ortigosa-Blanch, J. C. Knight, W. J. Wadsworth, B. J. Mangan, T. A. Birks, and P. S. J. Russell, "Highly birefringent photonic crystal fibers," *Opt. Lett.*, vol. 25, pp. 1325–1327, 2000.

[8] T. A. Birks, D. Mogilevtsev, J. C. Knight, and P. S. J. Russell, "Dispersion compensation using single material fibers," *IEEE Photon. Technol. Lett.*, vol. 11, no. 6, pp. 674–676, Jun. 1999.

[9] J. S. Wang, E. M. Vogel, and E. Snitzer, "Tellurite glass: A new candidate for fiber devices," *Opt. Mater.*, vol. 3, pp. 187–203, 1994.

[10] T. M. Monro, Y. D. West, D. W. Hewak, N. G. R. Broderick, and D. J. Richardson, "Chalcogenide holey fibers," *Electron. Lett.*, vol. 36, pp. 1998–2000, 2000.

[11] T. M. Monro, K. M. Kiang, J. H. Lee, K. Frampton, Z. Yusoff, R. Moore, J. Tucknott, D. W. Hewak, H. N. Rutt, and D. J. Richardson, "High nonlinearity extruded single-mode holey optical fibers," presented at the Optical Fiber Communication Conf., Anaheim, CA, Mar. 19–21, 2002, Postdeadline Paper FA1.

[12] P. Petropoulos, T. M. Monro, H. Ebendorff-Heidepriem, K. Frampton, R. C. Moore, H. N. Rutt, and D. J. Richardson, "Soliton-self-frequency-shift effects and pulse compression in an anomalously dispersive high nonlinearity lead silicate holey fiber," presented at the Optical Fiber Communication Conf., Atlanta, GA, Mar. 23–28, 2003, Postdeadline Paper PD03.

[13] V. V. Ravi Kanth Kumar, A. K. George, W. H. Reeves, J. C. Knight, P. S. J. Russell, F. G. Omenetto, and A. J. Taylor, "Extruded soft glass photonic crystal fiber for ultrabroad supercontinuum generation," *Opt. Express*, vol. 10, pp. 1520–1525, 2002.

[14] J. M. Pottage, D. M. Bird, T. D. Hedley, T. A. Birks, J. C. Knight, and P. S. J. Russell, "Robust photonic band gaps for hollow core guidance in PCF made from high index glass," *Opt. Express*, vol. 11, pp. 2854–2861, 2003.

[15] B. Temelkuran, S. D. Hart, G. Benoit, J. D. Joannopoulos, and Y. Fink, "Wavelength-scalable hollow optical fibers with large photonic bandgaps for CO_2 laser transmission," *Nature*, vol. 420, pp. 650–653, 2002.

[16] E. H. Fontana, "A versatile parallel-plate viscosimeter for glass viscosity measurements to 1000 °C," *Amer. Ceram. Soc. Bull.*, vol. 49, pp. 594–597, 1970.

[17] A. I. Markov, "Ultrasonic drilling and milling of hard nonmetallic materials with diamond tools," *Machine Tooling*, vol. 48, pp. 33–35, 1977.

[18] H. R. Lillie, "Viscosity time temperature relations in glass at annealing temperatures," *J. Amer. Ceram. Soc. Bull.*, vol. 16, pp. 619–631, 1933.

[19] D. Hewak, Ed., *Properties, Processing and Applications of Glass and Rare Earth-Doped Glasses for Optical Fibers*. ser. Emis Datareviews Series, no. 22. London, U.K.: IEE, 1998, ch. A2, pp. 25–34.

[20] H. Scholze, *Glass: Nature, Structure and Properties*. New York: Springer-Verlag, 1991, ch. 3.

[21] ——, "Der Einbau des Wassers in Glasern," *Glastechn. Ber.*, vol. 32, pp. 81–88, 1959.

[22] M. Cable, "Ch. 1: Classical Glass Technology," in *Materials Science and Technology, Vol. 9, Glasses and Amorphous Materials*, R. W. Cahn, P. Haasenm, and E. J. Kramer, Eds., 1991, vol. ed. J. Zarzycki, p. 2629.

[23] A. Schuster, "Radiation through a fogg atmosphere," *Astrophys. J.*, vol. 21, pp. 1–22, 1905.

[24] R. H. S. Winterton, *Heat Transfer*. Oxford, U.K.: Oxford Univ. Press, 1997, p. 81.

[25] T. D. Krauss and F. W. Wise, "Femtosecond measurement of nonlinear absorption and refraction in CdS, ZnSe, and ZnS," *Appl. Phys. Lett.*, vol. 65, pp. 1739–1741, 1994.

[26] I. Kang, T. D. Krauss, F. W. Wise, B. G. Aitken, and N. F. Borrelli, "Femtosecond measurement of enhanced optical nonlinearities of sulfide glasses and heavy-metal-doped oxide glasses," *J. Opt. Soc. Amer. B, Opt. Phys.*, vol. 12, pp. 2053–2059, 1995.

[27] N. L. Boiling, A. J. Glass, and A. Owyoung, "Empirical relationships for predicting nonlinear refractive index changes in optical solids," *IEEE J. Quantum. Electron.*, vol. QE-14, no. 8, pp. 601–608, Aug. 1978.

[28] J. M. Harbold, F. Q. Ilday, F. W. Wise, J. S. Sanghera, V. Q. Nguyen, I. B. Shaw, and I. D. Aggarwal, "Highly nonlinear As–S–Se glasses for all optical switching," *Opt. Lett.*, vol. 27, pp. 119–121, 2002.

[29] D. N. Nikogosyan, *Properties of Optical and Laser-Related Materials: A Handbook*. New York: Wiley, 1997, p. 181.

[30] H. Nasu, O. Sugimoto, J. Matsuoka, and K. Kamiya, "Non-resonant-type third-order optical nonlinearity of alkali silicate and alkali aluminosilicate glasses-contribution of individual chemical species in the glasses to $\chi(3)$," *J. Non-Cryst. Solids*, vol. 182, pp. 321–327, 1995.

[31] I. Thomazeau, J. Etchepare, G. Grillon, and A. Migus, "Electronic nonlinear optical susceptibilities of silicate glasses," *Opt. Lett.*, vol. 10, pp. 223–225, 1985.

[32] R. Adair, L. L. Chase, and S. A. Payne, "Nonlinear refractive index measurements of glasses of optical crystals," *Phys. Rev. B, Condens. Matter*, vol. 39, pp. 3337–3350, 1989.

[33] T. Kanamori, Y. Terunuma, and T. Miyashita, "Preparation of chalcogenide optical fiber," *Rev. Electr. Commun. Lab.*, vol. 32, pp. 469–477, 1984.

[34] M. Eijkelenborg, M. Large, A. Argyros, J. Zagari, S. Manos, N. A. Issa, I. M. Bassett, S. C. Fleming, R. C. McPhedran, C. M. de Sterke, and N. A. P. Nicorovici, "Microstructured polymer optical fiber," *Opt. Express*, vol. 9, pp. 319–327, 2001.

[35] E. Roeder, "Extrusion of glass," *J. Non-Cryst. Solid*, vol. 5, pp. 377–388, 1971.

[36] E. Yablonovitch, T. J. Gmitter, and K. M. Leung, "Photonic band structure: The face-centered-cubic case employing nonspherical atoms," *Phys. Rev. Lett.*, vol. 67, pp. 2295–2298, 1991.

[37] G. P. Agrawal, *Nonlinear Fiber Optics*. San Diego and London: Academic, 2001, ch. 2.

[38] X. Feng, T. M. Monro, P. Petropoulos, V. Finazzi, and D. Hewak, "Solid microstructured optical fiber," *Opt. Express*, vol. 11, pp. 2225–2230, 2003.

[39] J. C. Knight, T. A. Birks, P. S. J. Russell, and D. M. Atkin, "Errata: All silica single-mode fiber with photonic crystal cladding," *Opt. Lett.*, vol. 22, pp. 484–485, 1997.

Xian Feng, photograph and biography not available at the time of publication.

Arshad K. Mairaj, photograph and biography not available at the time of publication.

Daniel W. Hewak, photograph and biography not available at the time of publication.

Tanya M. Monro, photograph and biography not available at the time of publication.